Published in final edited form as:
Intravital. 2012 ; 1(1): . doi:10.4161/intv.21557.

Video-rate resonant scanning multiphoton microscopy:

An emerging technique for intravital imaging of the tumor microenvironment

Nathaniel D. Kirkpatrick[†], **Euiheon Chung**[†,‡], **Daniel C. Cook**[†], **Xiaoxing Han**, **Gabriel Gruionu**, **Shan Liao**, **Lance L. Munn**, **Timothy P. Padera**, **Dai Fukumura**, and **Rakesh K. Jain**[*]
Edwin L. Steele Laboratory for Tumor Biology; Department of Radiation Oncology; Massachusetts General Hospital; Harvard Medical School; Boston, MA USA

Abstract

The abnormal tumor microenvironment fuels tumor progression, metastasis, immune suppression, and treatment resistance. Over last several decades, developments in and applications of intravital microscopy have provided unprecedented insights into the dynamics of the tumor microenvironment. In particular, intravital multiphoton microscopy has revealed the abnormal structure and function of tumor-associated blood and lymphatic vessels, the role of aberrant tumor matrix in drug delivery, invasion and metastasis of tumor cells, the dynamics of immune cell trafficking to and within tumors, and gene expression in tumors. However, traditional multiphoton microscopy suffers from inherently slow imaging rates—only a few frames per second, thus unable to capture more rapid events such as blood flow, lymphatic flow, and cell movement within vessels. Here, we report the development and implementation of a video-rate multiphoton microscope (VR-MPLSM) based on resonant galvanometer mirror scanning that is capable of recording at 30 frames per second and acquiring intravital multispectral images. We show that the design of the system can be readily implemented and is adaptable to various experimental models. As examples, we demonstrate the utility of the system to directly measure flow within tumors, capture metastatic cancer cells moving within the brain vasculature and cells in lymphatic vessels, and image acute responses to changes in a vascular network. VR-MPLSM thus has the potential to further advance intravital imaging and provide new insight into the biology of the tumor microenvironment.

Keywords

video-rate; multiphoton; tumor microenvironment; vessels; metastasis; lymphatics

Introduction

Since its development two decades ago,[1] multiphoton laser scanning microscopy (MPLSM) has provided invaluable insight into biological processes. MPLSM is an optical imaging modality that uses near infrared, nonlinear excitation to produce a highly spatially localized

[*]Correspondence to: Rakesh K. Jain; jain@steele.mgh.harvard.edu.
[†]These authors contributed equally to this work.
[‡]Current affiliation: Gwangju Institute of Science and Technology; Gwangju, South Korea

Disclosure of Potential Conflicts of Interest
No potential conflicts of interest were disclosed.

Supplemental Material
Supplemental materials may be found here: www.landesbioscience.com/journals/epigenetics/article/21557

(subfemtoliter volume) fluorescence or scattering volume, thus providing intrinsic optical sectioning deep within biological tissue. MPLSM is particularly well suited to biological imaging, compared with conventional and confocal fluorescence microscopy, due to its relatively large penetration depths in tissue as well as lower risk of phototoxicity and photobleaching.[2,3]

The application of MPLSM to pre-clinical models of cancer has proven to be a powerful tool in the investigation of tumor-host interactions.[4–8] The abnormal tumor microenvironment not only actively promotes tumor progression and metastasis but also poses a barrier to the delivery and efficacy of therapeutics. MPLSM allows for in vivo longitudinal monitoring, and this approach has been used to study various aspects of the tumor microenvironment during tumor progression and metastasis including: (lymph)angiogenesis, tumor cell-extracellular matrix interactions, intra(extra)vasation, and drug delivery. Despite these significant advances, conventional multiphoton microscopes lack the temporal resolution to capture rapid biological events. Thus, the application of emerging video-rate multiphoton laser scanning microscope (VR-MPLSM) technology to intravital imaging will be an important advancement to capture and analyze the dynamic nature of tumors at the microsecond timescale.

This report demonstrates the application of VR-MPLSM to intravital imaging using a custom-built system that achieves video rate laser scanning with resonant galvanometer mirrors. This system can be readily adapted from traditional multiphoton microscope platforms. Additionally, we show that VR-MPLSM can be combined with a liquid crystal tunable filter (LCTF) to achieve spectral unmixing and distinguish colocalized, spectrally overlapping fluorophores. As a proof-of-concept, we demonstrate that our VR-MPLSM can directly measure blood flow within tumors, capture metastatic cancer cells moving within the brain vasculature as well as cells in lymphatic vessels, and image rapid blood flow alterations following selective vessel ablation. Additionally, we show that intravital multispectral imaging can be a valuable tool for high-flexibility selection and detection of multiple spectrally overlapping fluorophores.

Results

Microscope design and implementation

A number of approaches to VR-MPLSM have been described. These techniques include line scanning,[9] multifocal multiphoton microscopy (MMM),[10–13] acousto-optic deflectors scanning,[14,15] rotating polygonal scanning mirror[16,17] and resonant galvanometer driven mirrors.[18–20] Each video-rate microscope setup has its advantages and drawbacks, but the approach utilizing resonant galvanometer mirrors is particularly attractive given its similarity to conventional MPLSM setups. The primary difference with a resonant galvanometer is that by oscillating at its mechanical resonant frequency, it can overcome the limitation of mechanical inertia suffered by other galvanometer mirrors to achieve line scanning frequencies and video-rate frame rates. This approach, using both the forward and reverse sweeps of the resonant galvanometer, requires two corrections: (1) reversing the direction of every other line and (2) correcting the distortion at the edges of the images due to the sinusoidally varying velocity.[20]

We employed this resonant scanning technique by adapting the modified fixed stage upright BX51WI Olympus microscope body and using an 80 MHz, femtosecond pulsed Titanium:Sapphire laser as an excitation source (Fig. 1, see also Material and Methods for more details). Two orthogonally mounted galvanometer mirrors provide x-y (lateral) scanning of the laser beam. The driver boards for the mirrors as well as the circuits for generating the synchronization signals are housed within a custom-built scanning control

box (Sutter Instrument Co.). In addition, we included a motorized x-y stage (H101A ProScan II, Prior Scientific) for automated mosaic imaging for wide-area sampling, as well as a piezoelectric transducer (PZT) objective drive unit (PIFOC P-723.10, Physik Instrumente) for precise and rapid depth control during intravital imaging.

For generating images and videos, our system is capable of detecting up to 4 spectrally separated channels at either 30 or 60 frames/second. Images are captured and processed by the software package Video Savant® 4.0 (IO Industries, Inc.). The measured field of view, using a 20× Olympus physiology lens, is 315 × 295 μm.

In addition as a new feature to VR-MPLSMs, we provide a spectral deconvolution capability within our system using a liquid crystal tunable filter (LCTF) and the Nuance CCD camera by attaching this unit instead of PMT detectors. This allows us to spectrally separate both fluorescent tracers such as quantum dots and features such as pericytes and vessel lumens (Fig. 2). It would not be trivial to distinguish these two fluorophores with the conventional optical filters due to spectral overlap. With conventional laser-scanning fluorescence microscopes, the scanning mechanism is too slow to allow the Nuance CCD camera to acquire equal signal from every pixel for the duration of each individual spectral step. However, at longer acquisition times (~1,000 ms), the rapid frame rate of the video-rate microscope essentially mimics a bright field microscope and showed even illumination of the sample. These data show for the first time that multispectral imaging can be extended to intravital multi-photon microscopy.

To achieve rapid image collection in the VR-MPLSM, the cost is lower signal to noise ratio in order to maintain a high temporal resolution. Therefore, structural images can at times be difficult to interpret compared with regular MPLSM, especially small features such as individual cells (Fig. 3). To address this potential drawback, we employed frame averaging so that we could measure both fast dynamics in video-rate mode as well as high spatial resolution structural imaging with averaging mode (Fig. 3). A custom post-processing Matlab program allowed averaging and filtering to be selectively applied to individual channels.

Imaging changes in blood flow

The abnormal vascular network within tumors is a hallmark of tumor pathphysiology.[21–23] Tumor vessels are heterogeneous with regions of relatively high blood flow, intermittent and low blood flow, and even flow stasis.[24,25] Moreover, improving blood perfusion in tumors via vascular normalization confers therapeutic benefit in mouse models as well as cancer patients.[26,27] To further develop this strategy, it is critical to measure blood flow accurately in clinically relevant experimental tumor models and, to this end, intravital microscopy has been used extensively to measure tumor blood flow.[28,29] However, multiphoton microscopy, which can image deep into tumors at a high spatial resolution, suffers from poor temporal resolution and is unable to fully capture the three dimensional rapid flow of red blood cells.

Using the VR-MPLSM in a cranial window model, we examined the tumor blood flow in a brain tumor (U87 human glioblastoma). Following intravenous injection of tetramethylrhodamine-dextran (500 kDa), we observed abnormal blood flow throughout the tumor, with regions of low/intermittent, medium, and high flow (Fig. 4A–C; Video S1). To directly measure blood flow velocities, we labeled red blood cells with DiD membrane dye and imaged blood flow in tumors. We used a custom Matlab routine to analyze the flow of red blood cells in vessel segments by directly tracking the movement of individual red blood cells (Fig. 4D and E, see Material and Methods). When comparing vessels with similar diameters (< 20 μm), we found both higher and lower red blood cell velocities within the tumors compared with only high red blood cell velocities in the contra-lateral normal brain

providing support for a heterogeneous tumor blood flow distribution (Fig. 4F). With VR-MPLSM and this type of analysis, it is possible to directly map single vessel flow velocities throughout the tumor and quantify the effects of treatments on the vasculature over time.

To further illustrate the capability of the VR-MPLSM to detect temporal changes in blood flow, we imaged vessels with labeled red blood cells in the dorsal skinfold chamber.[30] Blood flow was altered by single vessel ablation and the VR-MPLSM was able to capture the change in flow dynamics in regions where vessels had been ablated (Fig. 5; Video S2). Thus, this technique is useful to investigate rapid changes in a vascular network, including settings of injury or shock.

Imaging tumor draining lymphatic vessels

Another critical aspect of the tumor microenvironment is the interaction between metastatic cancer cells and the local stroma. Cancer cells can invade and metastasize via lymphatic or blood vessels. In lymphatic metastasis, cancer cells travel through lymphatic vessels to the lymph nodes where they form lymphatic metastases. Intravital imaging has recently provided novel insights into the function of lymphatic valves.[31] However, little is known about how cells travel through the tumor-draining lymphatic vessel.[32]

Using the VR-MPLSM, we imaged the lymphatic vessels in mice bearing metastatic tumors (P008, mouse breast cancer). Despite the movement of the mouse and flow within the lymphatic vessels, we were able to vessel contraction and valve dynamics in the lymphatics (Fig. 6; Video S3). Clumps of red blood cells were observed next to lymphatic valves and they were intermittingly ejected through the lymphatic valve (Fig. 6; Video S3). It is interesting to note that cancer cells can travel as homotypic and/or heterotypic aggregates in blood and lymphatic vessels.[33] The ability of these aggregates to interact with these vessels may offer new insights into treatment of metastases.

Imaging brain metastasis

Blood vessels represent the more common route cancer cells use to disseminate to distant organs. MPLSM has recently been used to follow the growth of brain metastases in vivo.[34] However, one of the difficulties of imaging brain metastasis, particularly at an early stage, is localizing the cells that seed the vast network of vessels within the brain. Further, determining the dynamics of cell arrest in the brain vasculature is not possible with conventional microscopy. To determine the capability of the VR-MPLSM to follow brain metastases, we imaged cranial windows in mice that had just received intracardiac injections of GFP-labeled metastatic breast cancer cells (MDA-MB-231, human breast cancer). The VR-MPLSM allowed us to scan rapidly throughout the brain to image blood vessels, blood flow, and hematogenously disseminating cancer cells arrested within vessels (Fig. 7; Video S4). This application allows not only for imaging throughout large regions of the brain but also to determine the interaction between blood vessels and cancer cells at the earliest stage of brain metastasis.

Discussion

We have illustrated the use of VR-MPLSM in imaging multiple dynamic events in the tumor microenvironment and metastasis. In addition to blood flow, lymphatic function, and brain metastasis, there are many other potential applications for the VR-MPSLM in intravital imaging. Recent studies show the critical role of the immune system in tumor progression.[35–38] The VR-MPSLM has the potential to follow immune cells trafficking to tumors and capture the dynamic interaction between immune cells and their local microenvironment.

In addition to advantages in imaging dynamic biological events, the VR-MPLSM is able to limit imaging artifacts that are often caused by animal motion during in vivo imaging. For example, when imaging lymphatic vessels, muscle movement and blood vessel fluctuations can cause shifts in the lymphatic vessel. The VR-MPLSM can capture these macro movements of larger structures while still imaging the micro movements of cells.

Finally, the application of multispectral imaging techniques to VR-MPLSM has the potential to enable more sensitive quantitation of fluorescence signal in intravital microscopy experiments, particularly when multiple colocalized fluorescence labels are used that have overlapping emission spectra. Our system, specifically, could be used to accurately study the morphology of the tumor microenvironment using up to five or more fluorescence probes with the multispectral imaging and could potentially be combined with an independent analysis using the video-rate capabilities of the microscope in its conventional setup.

In summary, the application of VR-MPLSM for real-time intravital imaging and the capability for multispectral imaging provides unprecedented flexibility for in vivo fluorescence studies of tumor biology, and this approach has the capability to open new avenues of future research.

Materials and Methods

Microscope design

The video-rate multiphoton microscope platform is a modified fixed stage upright research microscope (BX51WI, Olympus). A side laser port allows entry of the excitation light. A motorized x-y stage (H101A ProScan II, Prior Scientific) is mounted for convenient and precise translations of the specimen, and a piezoelectric transducer (PZT) objective drive unit (PIFOC P-723.10, Physik Instrumente), with a range of 350 μm and a minimum displacement of 3.33 nm, is used for precision control of the axial position, thereby allowing the automated adjustment of imaging depth. The Olympus camera port is used to mount the dichroic mirrors and support the detectors. The upright microscope and optical elements are mounted on a 4′ by 4′ by 8″ optical table (Technical Manufacturing Corp.) while the laser is located on a separate optical table.

The excitation light is provided by a Titanium:Sapphire laser (pulse width < 100 fs, repetition rate 80 MHz), tunable in wavelength from the red to near-infrared spectrum (approximately 700 to 1,000 nm) with an average power output of approximately 2.50 Watts (Mai Tai, Spectra Physics, now Newport Corp.). The laser beam is guided by a series of mirrors through an adjustable neutral density (ND) filter (Newport Corp.), allowing easy adjustment of the beam power. An optical power meter (Newport Corp.) can be slid into place behind the ND filter to measure the power of the beam after attenuation. The beam is then deflected up to the level of the upright microscope's laser port via a periscope, which steers the excitation light onto the scanning mirrors.

The beam is scanned by two orthogonally mounted galvanometer mirrors. The driver boards for the mirrors as well as the circuits for generating the synchronization signals are housed within a custom-built scanning control box (Sutter Instrument Co.). The scanning control electronics, as described by Sanderson and Parker,[39] coordinate the movements of both mirrors and the timing of the sync signals that allow the frame acquisition hardware to map the pixel intensities. Vertical deflection is achieved with a standard galvanometer (M3S; GSI Lumonics) driven by a sawtooth waveform with a frequency of 30.95 (~30) or 61.89 (~60) Hz, thus providing frames at video-rate or twice as fast. Increasing the frame rate comes at the expense of decreasing the number of lines per frame by a factor of two, decreasing overall field of view. The faster horizontal deflection is achieved with a resonant

galvanometer (Counter Rotating Scanning Mirror, CRS; GSI Lumonics) that oscillates at 7.895 kHz (~8 kHz),[20] thus completing one forward or backward sweep in 63.3 μs. The periods of the standard and resonant galvanometer dictate a nominal total of 512 lines per frame at 30 Hz and 256 lines per frame at 60 Hz. The scanning electronics drive the two mirrors such that the vertical mirror is displaced by an angle equivalent to one line at every change in direction of the horizontal mirror. Thus, a raster pattern is generated in which the direction of horizontal scanning reverses with every line.

The scanning mirrors deflect the beam through a pupil lens and tube lens that are spaced apart a distance equal to the sum of their focal lengths to make the beam telecentric. The beam is directed to the objective lens by a short-pass dichromatic (dichroic) mirror (700 dcspxr, Chroma Technology Corp.). The objective lens (XLUMPFL20x W/IR Objective, Olympus) has a relatively low magnification (20×), high numerical aperture (NA = 0.95), and long working distance (2.0 mm), making it an optimal choice for intravital two-photon microscopy.

Fluorescence wavelengths are separated by a series of long-pass dichroics with increasingly larger cut-off wavelengths (485 nm, 565 nm and 650 nm; Chroma Technology Corp.). The mirrors are housed in modular cubes to allow the convenient swapping of the dichroic mirrors as necessitated by the fluorophores used. A band-pass filter (emission filter) is placed in front of each detector to minimize cross-talk of the fluorescence signal among the detectors.

Up to four PMT detectors (R5929 multialkali, head-on type, Hammamatsu Corp.) can be used at one time. The PMT cables connect to a 62-pin connector (CAB-DEV-ANV4, Bitflow, Inc.) that mates with the acquisition board of the computer. A frame grabber, the Alta-PCE-AN4 (Bitflow™ Inc.), converts the analog input of the PMTs into a digitized image, and a software package, Video Savant® 4.0 (IO Industries, Inc.), acts as an interface between the frame grabber and computer storage and enables real-time display.

The Alta-PCE-AN4 has four virtual frame grabbers (VFGs), each with three analog-to-digital converters (DACs) and can consequently support up to four independent sets of fluorescence and synchronization (sync) signals. The Bitflow Software Development Kit (SDK) provides several configuration utilities which are used to select the camera file, adjust how the image is captured, and display the images as they are received by the frame grabber in real-time.

Video Savant processes the images from the frame grabber and writes them to the hard drive. A custom written filter included in the Video Savant package performs the distortion correction algorithm.

Multispectral imaging

For multispectral imaging capability, the Nuance system (CRI) was mounted onto the Olympus camera port. The Nuance has a range of 500 to 950 nm, narrow (8 nm) acquisition spectral bandwidths that can be sequentially shifted, and dedicated software that enables semi-automated spectral unmixing.

Intravital imaging experiments

All animal procedures were performed following the guidelines of the Public Health Service Policy on the Humane Care of Laboratory Animals and approved by the Institutional Animal Care and Use Committee of Massachusetts General Hospital.

Tumors were grown in either the cranial window of mice (U87 GFP) or in the leg of mice (P008) and imaged as previously described.[5,31]

For red blood cell imaging, mice were injected intraveneously with 200 μl of red blood cells (RBCs) labeled with 1,1-diocta-decyl-3,3,3,3-tetramethylindodicarbocyanine perchlorate (DiD; Invitrogen), a far-red fluorescent dye. The RBCs were prepared by centrifuging to separate the RBCs from the plasma and leukocytes and performing two cycles of 1:100 dilution with phosphate buffered saline (PBS) and room temperature incubation with 1 mg/ml DiD.[29] For vascular angiography, 100 μl of 1 mg/ mL rhodamine-Dextran was injected intravenously. For lymphangiography, 5 μl of 2.5 mg/mL FITC-Dextran was injected subcutaneously.

Image processing for red blood cell velocities

To determine the velocity of red blood cells traveling within a given vessel or region of a vessel, a custom-written Matlab program was used. This program reads in a video as a post-processed multi-page TIFF. The program displays the first frame of the video, and the user marks the blood vessels or regions of interest by interactively drawing a polygon around its borders. The user draws several well-spaced lines perpendicularly across the vessel within the marked region to calculate the average diameter. Any number of regions may be defined and any number of diameter-measuring lines may be placed therein. It should be noted that placing more lines will increase the accuracy of the diameter measurement, and, in that case that the diameter varies appreciably within the region, the standard deviation will provide a measure of this variation in diameter. The marked frame, with a textbox indicating the index of each ROI, is saved as a Matlab figure file to the current directory for future reference.

When the user has found a frame range in which a cell moves through one of the specified regions, the program switches into “trajectory mode.” The cursor over the selection window becomes a crosshair, and the user clicks on the cell of interest. The selection window will then display the next frame, and the reference window will show the previous frame from the selection window with a green dot indicating the location of the mouse click. The locations of the selected pixels are saved and used to find the velocity of the trajectory. Once the cell has moved outside the ROI, the user exits trajectory mode. The program assigns the trajectory an index and calculates the average velocity of the cell, the standard deviation of the velocity, and the relative standard deviation. Velocities are calculated from the distance traveled by the cell, the frame rate, and the number of frames that elapsed. Any number of trajectories may be analyzed.

Supplementary Material

Refer to Web version on PubMed Central for supplementary material.

Acknowledgments

The authors would like to thank Julia Kahn and Sylvie Roberge for assistance with animal models. This work was supported by NIH 2P01CA080124–11A1 (R.K.J.), NIH 5R01CA126642–05 (R.K.J.), DOD CDMRP BC095991 (R.K.J.), NIH 5R01CA096915–10 (D.F.), NIH 5R01CA149285–03 (L.L.M.), NIH 1DP2OD008780–01 (T.P.P.), NIH T32 CA073479 (N.D.K., G.G.), NIH R00CA137167 (T.P.P.), Basic Research Projects in High-tech Industrial Technology by GIST (E.C.), the National Research Foundation of Korea the Basic Science Research Program 2012R1A1A1012853 (E.C.), the Bio & Medical Technology Development Program 2011-0019619 and 2011-0019632 (E.C.) and the Tosteson postdoctoral fellowship (E.C.). R.K.J. has research grants from Dyax, MedImmune and Roche; serves as a consultant to Noxxon Pharmaceuticals; serves on the Scientific Advisory Board of Enlight and SynDevRx; serves on the Board of Directors of XTuit; serves on the Board of H&Q Healthcare Investors and H&Q Life Sciences Investors; and has equity in Enlight, SynDevRx and XTuit Pharmaceuticals. No funds or reagents from any of these organizations were used in the current study. Therefore, there are no conflicts of interest.

References

1. Denk W, Strickler JH, Webb WW. Two-photon scanning fluorescence microscopy. Science. 1990; 248:73–6. http://dx.doi.org/10.1126/science.2321027. [PubMed: 2321027]
2. Helmchen F, Denk W. Deep tissue two-photon microscopy. Nat Methods. 2005; 2:932–40. http://dx.doi.org/10.1038/nmeth818. [PubMed: 16299478]
3. Zipfel WR, Williams RM, Webb WW. Nonlinear magic: multiphoton microscopy in the biosciences. Nat Biotechnol. 2003; 21:1369–77. http://dx.doi.org/10.1038/nbt899. [PubMed: 14595365]
4. Padera TP, Stoll BR, Tooredman JB, Capen D, di Tomaso E, Jain RK. Pathology: cancer cells compress intratumour vessels. Nature. 2004; 427:695. http://dx.doi.org/10.1038/427695a. [PubMed: 14973470]
5. Kamoun WS, Ley CD, Farrar CT, Duyverman AM, Lahdenranta J, Lacorre DA, et al. Edema control by cediranib, a vascular endothelial growth factor receptor-targeted kinase inhibitor, prolongs survival despite persistent brain tumor growth in mice. J Clin Oncol. 2009; 27:2542–52. http://dx.doi.org/10.1200/JCO.2008.19.9356. [PubMed: 19332720]
6. Brown EB, Campbell RB, Tsuzuki Y, Xu L, Carmeliet P, Fukumura D, et al. In vivo measurement of gene expression, angiogenesis and physiological function in tumors using multiphoton laser scanning microscopy. Nat Med. 2001; 7:864–8. http://dx.doi.org/10.1038/89997. [PubMed: 11433354]
7. Brown E, McKee T, di Tomaso E, Pluen A, Seed B, Boucher Y, et al. Dynamic imaging of collagen and its modulation in tumors in vivo using second-harmonic generation. Nat Med. 2003; 9:796–800. http://dx.doi.org/10.1038/nm879. [PubMed: 12754503]
8. Stroh M, Zimmer JP, Duda DG, Levchenko TS, Cohen KS, Brown EB, et al. Quantum dots spectrally distinguish multiple species within the tumor milieu in vivo. Nat Med. 2005; 11:678–82. http://dx.doi.org/10.1038/nm1247. [PubMed: 15880117]
9. Brakenhoff GJ, Squier J, Norris T, Bliton AC, Wade MH, Athey B. Real-time two-photon confocal microscopy using a femtosecond, amplified Ti:sapphire system. J Microsc. 1996; 181:253–9. http://dx.doi.org/10.1046/j.1365-2818.1996.97379.x. [PubMed: 8642584]
10. Bewersdorf J, Pick R, Hell SW. Multifocal multiphoton microscopy. Opt Lett. 1998; 23:655–7. http://dx.doi.org/10.1364/OL.23.000655. [PubMed: 18087301]
11. Buist AH, Müller M, Squier JBGJ. Real time two-photon absorption microscopy using multi point excitation. J Microsc. 1998; 192:217–26. http://dx.doi.org/10.1046/j.1365-2818.1998.00431.x.
12. Straub M, Lodemann P, Holroyd P, Jahn R, Hell SW. Live cell imaging by multifocal multiphoton microscopy. Eur J Cell Biol. 2000; 79:726–34. http://dx.doi.org/10.1078/0171-9335-00105. [PubMed: 11089921]
13. Andresen V, Egner A, Hell SW. Time-multiplexed multifocal multiphoton microscope. Opt Lett. 2001; 26:75–7. http://dx.doi.org/10.1364/OL.26.000075. [PubMed: 18033511]
14. Iyer V, Losavio BE, Saggau P. Compensation of spatial and temporal dispersion for acousto-optic multiphoton laser-scanning microscopy. J Biomed Opt. 2003; 8:460–71. http://dx.doi.org/10.1117/1.1580827. [PubMed: 12880352]
15. Salomé R, Kremer Y, Dieudonné S, Léger JF, Krichevsky O, Wyart C, et al. Ultrafast random-access laser scanning in two-photon microscopy using acousto-optic deflectors. J Neurosci Methods. 2006; 154:161–74. http://dx.doi.org/10.1016/j.jneumeth.2005.12.010. [PubMed: 16458361]
16. Kim KH, Buehler C, So PTC. High-speed, two-photon scanning microscope. Appl Opt. 1999; 38:6004-9. http://dx.doi.org/10.1364/AO.38.006004. [PubMed: 18324120]
17. Kim KH, Buehler C, Dong CY, Masters BR, So PTC. Tissue imaging using two-photon vide rate microscope. Proc SPIE. 1999; 3604:60–6. http://dx.doi.org/10.1117/12.349216.
18. Nguyen QT, Callamaras N, Hsieh C, Parker I. Construction of a two-photon microscope for video-rate Ca(2+) imaging. Cell Calcium. 2001; 30:383–93. http://dx.doi.org/10.1054/ceca.2001.0246. [PubMed: 11728133]

19. Fan GY, Fujisaki H, Miyawaki A, Tsay RK, Tsien RY, Ellisman MH. Video-rate scanning two-photon excitation fluorescence microscopy and ratio imaging with cameleons. Biophys J. 1999; 76:2412–20. http://dx.doi.org/10.1016/S0006-3495(99)77396-0. [PubMed: 10233058]
20. Sanderson MJ. Acquisition of Multiple Real-Time Images for Laser Scanning Microscopy. Microscopy and Analysis. 2004; 18:17–23.
21. Jain RK. Normalization of tumor vasculature: an emerging concept in antiangiogenic therapy. Science. 2005; 307:58–62. http://dx.doi.org/10.1126/science.1104819. [PubMed: 15637262]
22. Carmeliet P, Jain RK. Principles and mechanisms of vessel normalization for cancer and other angiogenic diseases. Nat Rev Drug Discov. 2011; 10:417–27. http://dx.doi.org/10.1038/nrd3455. [PubMed: 21629292]
23. Goel S, Duda DG, Xu L, Munn LL, Boucher Y, Fukumura D, et al. Normalization of the vasculature for treatment of cancer and other diseases. Physiol Rev. 2011; 91:1071–121. http://dx.doi.org/10.1152/physrev.00038.2010. [PubMed: 21742796]
24. Jain RK. Determinants of tumor blood flow: a review. Cancer Res. 1988; 48:2641–58. [PubMed: 3282647]
25. Endrich B, Zweifach BW, Reinhold HS, Intaglietta M. Quantitative studies of microcirculatory function in malignant tissue: influence of temperature on microvascular hemodynamics during the early growth of the BA 1112 rat sarcoma. Int J Radiat Oncol Biol Phys. 1979; 5:2021–30. http://dx.doi.org/10.1016/0360-3016(79)90954-4. [PubMed: 544581]
26. Winkler F, Kozin SV, Tong RT, Chae SS, Booth MF, Garkavtsev I, et al. Kinetics of vascular normalization by VEGFR2 blockade governs brain tumor response to radiation: role of oxygenation, angiopoietin-1, and matrix metalloproteinases. Cancer Cell. 2004; 6:553–63. [PubMed: 15607960]
27. Sorensen AG, Emblem KE, Polaskova P, Jennings D, Kim H, Ancukiewicz M, et al. Increased survival of glioblastoma patients who respond to antiangiogenic therapy with elevated blood perfusion. Cancer Res. 2012; 72:402–7. http://dx.doi.org/10.1158/0008-5472.CAN-11-2464. [PubMed: 22127927]
28. Jain RK, Munn LL, Fukumura D. Dissecting tumour pathophysiology using intravital microscopy. Nat Rev Cancer. 2002; 2:266–76. http://dx.doi.org/10.1038/nrc778. [PubMed: 12001988]
29. Kamoun WS, Chae SS, Lacorre DA, Tyrrell JA, Mitre M, Gillissen MA, et al. Simultaneous measurement of RBC velocity, flux, hematocrit and shear rate in vascular networks. Nat Methods. 2010; 7:655–60. http://dx.doi.org/10.1038/nmeth.1475. [PubMed: 20581828]
30. Leunig M, Yuan F, Menger MD, Boucher Y, Goetz AE, Messmer K, et al. Angiogenesis, microvascular architecture, microhemodynamics, and interstitial fluid pressure during early growth of human adenocarcinoma LS174T in SCID mice. Cancer Res. 1992; 52:6553–60. [PubMed: 1384965]
31. Liao S, Cheng G, Conner DA, Huang Y, Kucherlapati RS, Munn LL, et al. Impaired lymphatic contraction associated with immunosuppression. Proc Natl Acad Sci U S A. 2011; 108:18784–9. http://dx.doi.org/10.1073/pnas.1116152108. [PubMed: 22065738]
32. Hoshida T, Isaka N, Hagendoorn J, di Tomaso E, Chen YL, Pytowski B, et al. Imaging steps of lymphatic metastasis reveals that vascular endothelial growth factor-C increases metastasis by increasing delivery of cancer cells to lymph nodes: therapeutic implications. Cancer Res. 2006; 66:8065–75. http://dx.doi.org/10.1158/0008-5472.CAN-06-1392. [PubMed: 16912183]
33. Duda DG, Duyverman AM, Kohno M, Snuderl M, Steller EJ, Fukumura D, et al. Malignant cells facilitate lung metastasis by bringing their own soil. Proc Natl Acad Sci U S A. 2010; 107:21677–82. http://dx.doi.org/10.1073/pnas.1016234107. [PubMed: 21098274]
34. Kienast Y, von Baumgarten L, Fuhrmann M, Klinkert WEF, Goldbrunner R, Herms J, et al. Real-time imaging reveals the single steps of brain metastasis formation. Nat Med. 2010; 16:116–22. http://dx.doi.org/10.1038/nm.2072. [PubMed: 20023634]
35. Shiao SL, Ganesan AP, Rugo HS, Coussens LM. Immune microenvironments in solid tumors: new targets for therapy. Genes Dev. 2011; 25:2559–72. http://dx.doi.org/10.1101/gad.169029.111. [PubMed: 22190457]
36. DeNardo DG, Brennan DJ, Rexhepaj E, Ruffell B, Shiao SL, Madden SF, et al. Leukocyte complexity predicts breast cancer survival and functionally regulates response to chemotherapy.

Cancer Discov. 2011; 1:54–67. http://dx.doi.org/10.1158/2159-8274.CD-10-0028. [PubMed: 22039576]

37. Qian BZ, Pollard JW. Macrophage diversity enhances tumor progression and metastasis. Cell. 2010; 141:39–51. http://dx.doi.org/10.1016/j.cell.2010.03.014. [PubMed: 20371344]
38. Wyckoff JB, Wang Y, Lin EY, Li JF, Goswami S, Stanley ER, et al. Direct visualization of macrophage-assisted tumor cell intravasation in mammary tumors. Cancer Res. 2007; 67:2649–56. http://dx.doi.org/10.1158/0008-5472.CAN-06-1823. [PubMed: 17363585]
39. Sanderson MJ, Parker I. Video-rate confocal microscopy. Methods Enzymol. 2003; 360:447–81. http://dx.doi.org/10.1016/S0076-6879(03)60123-0. [PubMed: 12622163]

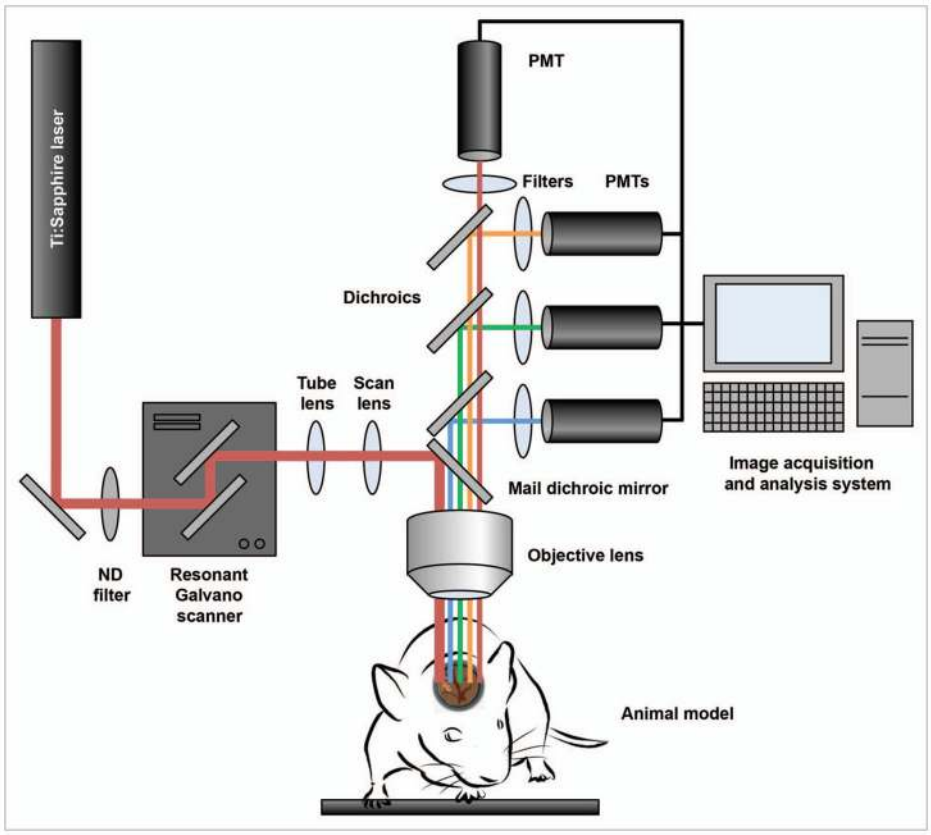

Figure 1.
Video-rate multiphoton laser scanning microscope system layout. The microscope setup is similar to other multiphoton laser scanning systems with one notable difference: resonant scanning mirrors scan the laser across the specimen at video-rate speeds. The system is equipped with 4 non-descanned PMT based detectors for 4-channel imaging or alternatively the detectors can be replaced by the Nuance system for multispectral imaging. In order to scan tissue rapidly in both the axial and vertical directions, the system is also fitted with an automated x-y stage and a piezoelectric controlled z-focus.

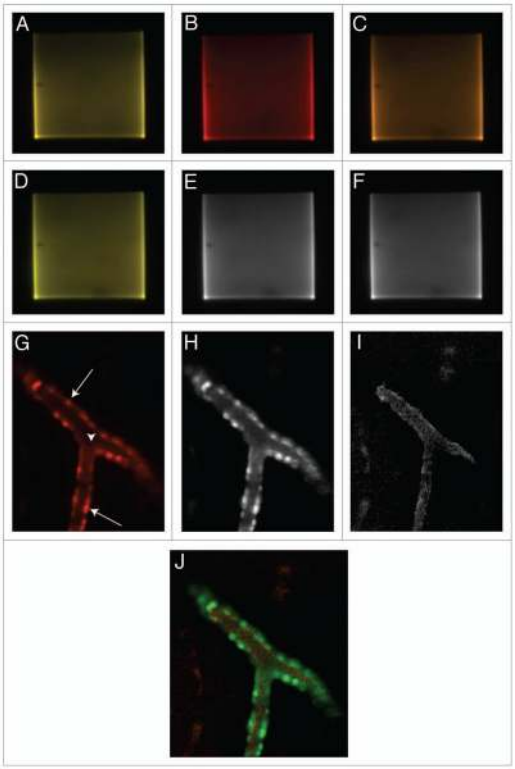

Figure 2.

Intravital multispectral imaging with the VR-MPLSM combined with the Nuance multispectral camera. Each image was acquired at 1,000 ms exposures using 10 nm steps over a spectral range of 530 to 630 nm and a laser excitation of 840 nm with 20 mW of power incident on the sample. (A) Solutions of 570 nm quantum dots (yellow color) and (B) 602 nm quantum dots (red color) were imaged separately. Each is shown in true color based on the wavelength range measured with the Nuance system. (C) A 1:1 mixture of the 570 nm and 602 nm quantum dots was imaged and is shown in true color (orange). (D) The Nuance system also created a false-colored composite based on the contribution of two different spectral profiles. This composite can readily unmixed into the contribution of the individual quantum dots as shown in grayscale for the (E) 570 nm and (F) 602 nm quantum dots. To demonstrate that spectral unmixing was also possible in intravital imaging, αSMA dsRed transgenic mice were injected with rhodamine-dextran. (G) A true-color image shows both dsRed perivascular cells (arrows) and rhodamine dextran in the vessel lumen (arrowhead). The similarity of these spectra is readily apparent, and they would thus be difficult to distinguish spectrally via conventional laser-scanning multiphoton microscopy. DsRed (H) and rhodamine (I) were spectrally separated and a composite image (J) was generated with rhodamine false-colored red and the DsRed labeled pericytes false-colored green.

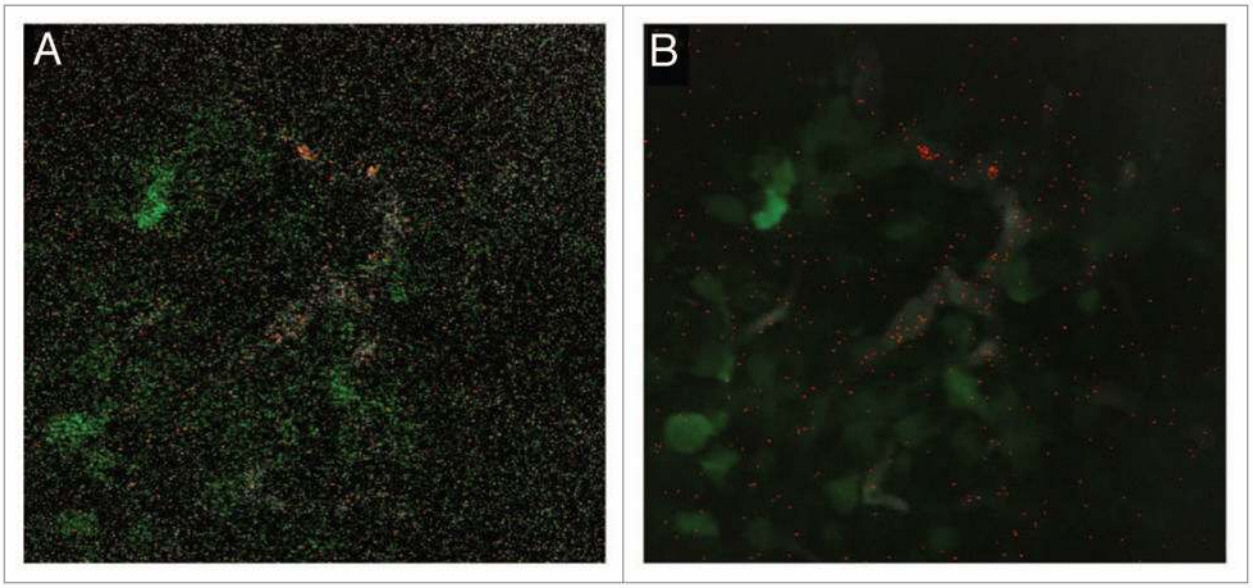

Figure 3.
Frame averaging to improve signal to noise. (A) At times the rapid collection of images results in noisy images (tumor cells, green; blood vessels, grayscale; quantum dots, red). (B) With frame averaging, these images can be cleaned up and features more easily distinguishable.

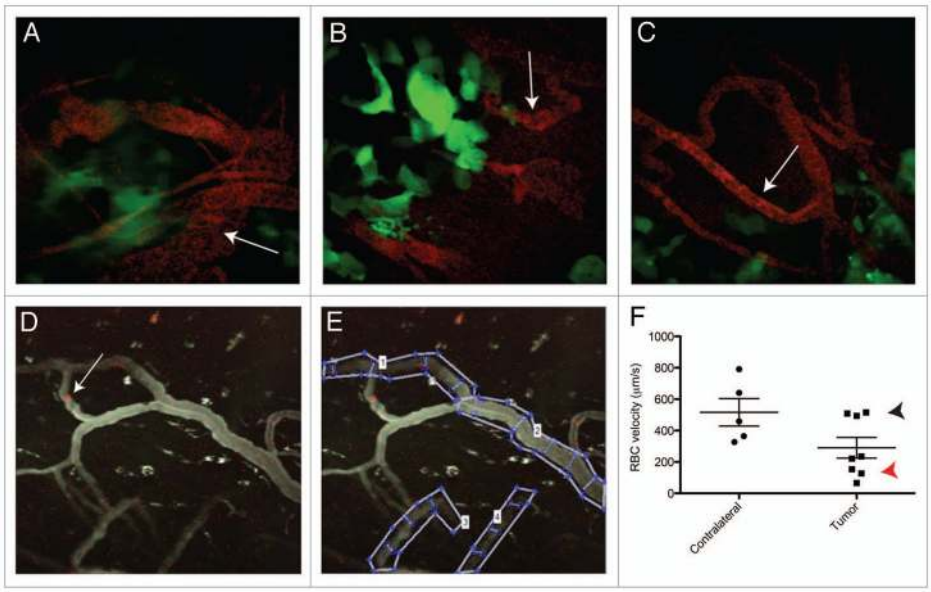

Figure 4.

Imaging tumor blood flow. Mice bearing U87-GFP brain tumors were injected with rhodamine dextran. (A) Large tumor vessels exhibited slow flow (arrow) while other regions showed areas of (B) intermediate (arrow) and (C) high flow (arrow). Tumor cells, green; blood vessels, red). See also Video S1. (D) Blood flow was measured with labeled red blood cells (red, arrow) and (E) vessels were segmented into regions for analysis with a custom Matlab program enabling semi-automated RBC tracing to determine flow velocity within selected vessels. (F) Quantification of blood flow velocities in vessels 20 μm in diameter or less shows a heterogeneous distribution of flow velocities within tumors with both high (black arrowhead) and low velocities (red arrowhead). In contrast, vessels from the contralateral normal brain all exhibited higher red blood cell velocities. Each point represents a vessel segment. Standard error bars are shown.

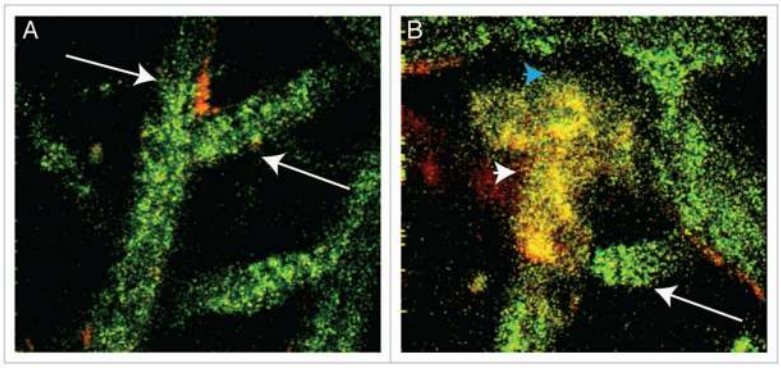

Figure 5.

Imaging rapid changes in blood flow. aSMA dsRed positive perivascular cells (red) outline a vessel with (A) a high flux of labeled red blood cells in vessels at a branch point (green, arrows). (B) Following ablation of the upper branch of the vessel (white arrowhead), all blood flow stopped in the upper branch (blue arrowhead) and was shunted to the lower branch of the vessel (arrow). An average of 10 frames is shown. See also Video S2 to observe flow of individual red blood cells and changes in flow to surrounding vessels.

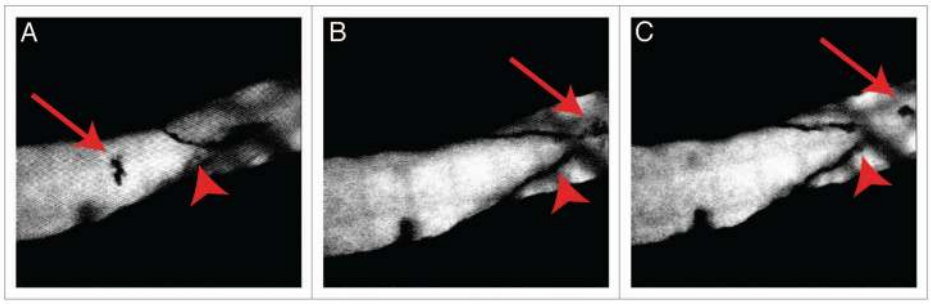

Figure 6.

Imaging cells in tumor draining lymphatic vessels. Lymphatic vessels were visualized with lymphangiography using FITC-dextran. (A) An aggregate of red blood cells (arrow) was observed in the lymphatic vessel near a lymphatic valve (arrowhead). The cell clump then (B) squeezed through the lymphatic valve and (C) ejected through the valve into the next lymphatic vessel segment. See also Video S3.

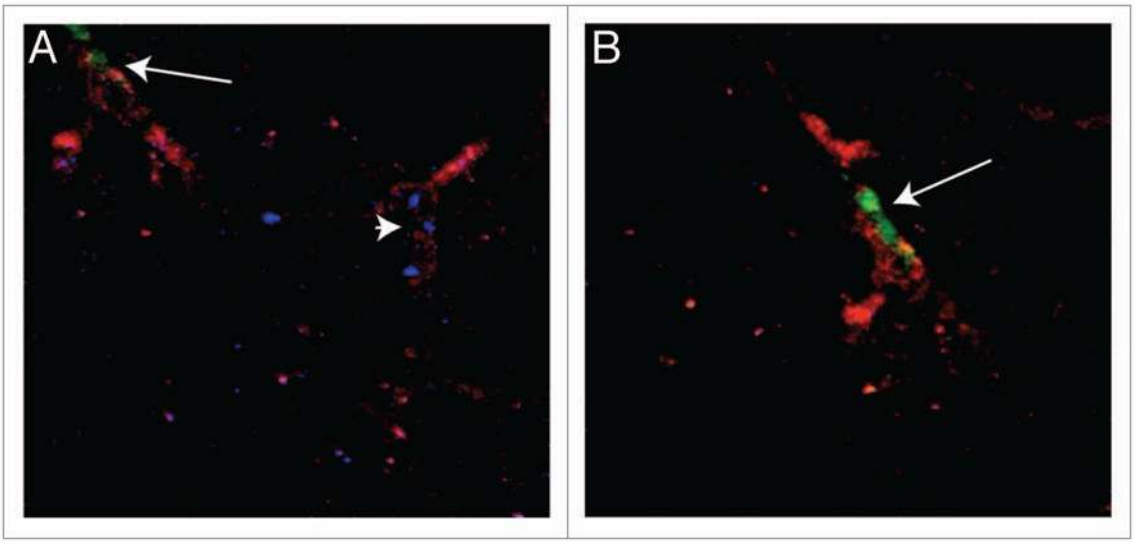

Figure 7.
Imaging cancer cell metastasis in the brain. (A) Scanning through brain vessels (red, rhodamine-dextran; blue, red blood cells) revealed areas of high flow (arrowhead) and cancer cells within vessels (arrow, green, GFP cancer cells) (B) The fast scanning capability of the VR-MPLSM allowed for rapid movement through the brain to localize cancer cells arrested inside vessels (arrow). See also Video S4.